2016-01-0705
Published 04/05/2016

doi:10.4271/2016-01-0705
saefuel.saejournals.org

Knock Resistance and Fine Particle Emissions for Several Biomass-Derived Oxygenates in a Direct-Injection Spark-Ignition Engine

Matthew A. Ratcliff, Jonathan Burton, Petr Sindler, Earl Christensen, Lisa Fouts, Gina M. Chupka, and Robert L. McCormick
National Renewable Energy Laboratory

ABSTRACT

Several high octane number oxygenates that could be derived from biomass were blended with gasoline and examined for performance properties and their impact on knock resistance and fine particle emissions in a single cylinder direct-injection spark-ignition engine. The oxygenates included ethanol, isobutanol, anisole, 4-methylanisole, 2-phenylethanol, 2,5-dimethyl furan, and 2,4-xylenol. These were blended into a summertime blendstock for oxygenate blending at levels ranging from 10 to 50 percent by volume. The base gasoline, its blends with p-xylene and p-cymene, and high-octane racing gasoline were tested as controls. Relevant gasoline properties including research octane number (RON), motor octane number, distillation curve, and vapor pressure were measured. Detailed hydrocarbon analysis was used to estimate heat of vaporization and particulate matter index (PMI). Experiments were conducted to measure knock-limited spark advance and particulate matter (PM) emissions. The results show a range of knock resistances that correlate well with RON. Molecules with relatively low boiling point and high vapor pressure had little effect on PM emissions. In contrast, the aromatic oxygenates caused significant increases in PM emissions (factors of 2 to 5) relative to the base gasoline. Thus, any effect of their oxygen atom on increasing local air-fuel ratio was outweighed by their low vapor pressure and high double-bond equivalent values. For most fuels and oxygenate blend components, PMI was a good predictor of PM emissions. However, the high boiling point, low vapor pressure oxygenates 2-phenylethanol and 2,4-xylenol produced lower PM emissions than predicted by PMI. This was likely because they did not fully evaporate and combust, and instead were swept into the lube oil.

CITATION: Ratcliff, M., Burton, J., Sindler, P., Christensen, E. et al., "Knock Resistance and Fine Particle Emissions for Several Biomass-Derived Oxygenates in a Direct-Injection Spark-Ignition Engine," *SAE Int. J. Fuels Lubr.* 9(1):2016, doi:10.4271/2016-01-0705.

INTRODUCTION

A number of factors are currently converging to compel significant changes in automobile spark-ignition (SI) fuel and engine technology. Concerns regarding global climate change caused by greenhouse gas emissions [1] are leading to legislation in many countries mandating the use of low-net carbon emission fuels, primarily biofuels [2]. In the United States, for example, renewable fuel usage is mandated to increase under the Renewable Fuel Standard [3]. The same climate change concerns are driving the introduction of more stringent standards for fuel economy as well as greenhouse gas emissions at the tailpipe [4]; this in turn is driving research to increase the efficiency of SI engines. High-efficiency SI engines will apply a number of different technologies, including direct injection (DI), which takes advantage of evaporative cooling of the intake charge to reduce engine knock, allowing an increase in boost pressure and/or compression ratio [5]. Further increases in boost pressure and compression ratio (and consequently efficiency) require use of more highly knock-resistant fuel to maintain optimal or near optimal combustion phasing.

The ability of an SI engine fuel to resist autoignition and avoid knock is measured as octane number, a critical performance parameter for SI engines. In the United States, the octane number used for retail gasoline is the anti-knock index, which is the average of the research octane number (RON) (ASTM D2699-13b) and motor octane number (MON) (ASTM D2700-13b). The primary differences between the RON and MON measurements are intake charge temperature and engine speed, with the RON test using a significantly lower (and variable) intake charge temperature and 600 revolutions per minute (rpm) engine speed, while the MON test is conducted at a much higher, fixed intake charge temperature and 900 rpm engine speed. Recent studies have demonstrated that in modern engines increasing MON at constant RON may actually lower the fuel knock resistance [6]. Octane sensitivity (S), the difference between RON and MON (S = RON - MON), can be interpreted as the sensitivity of the fuel autoignition kinetics to the temperature of the unburned end-gas [7]. Kalghatgi [8] and Mittal and co-workers [9] have shown that fuels with higher S have slower autoignition kinetics at lower temperatures than do fuels with lower S. They show that for modern engines, a more meaningful octane index (OI), compared to anti-knock index, is:

$$OI = RON - K \times S \quad (1)$$

where K is a function of the temperature-pressure history that the fuel-air mixture experiences in the engine and is therefore different at different engine operating conditions. However, for specifying knock resistance in terms of OI, values of K at the most knock-limited low-speed, high-load conditions are most relevant. In boosted direct-injection spark-ignition (DISI) engines at low speed and high load, K is negative, consistent with the fact that fuels with higher octane sensitivity give higher knock resistance [10].

DISI engines can show substantially higher particulate matter (PM) emissions, on both a mass and particle number (PN) basis, compared to earlier technology port fuel injection engines [11, 12, 13, 14]. Because of the negative health impacts of fine particles [15] and the contribution of soot particles to global warming [16] regulatory agencies are putting into place large reductions in allowable levels of PM emissions for future model years [17, 18, 19]. Increased PM emissions from DISI engines are caused by diffusion combustion in locally rich regions. This can occur because of incomplete fuel spray breakup and evaporation, as well as impingement of the fuel spray on the piston or cylinder wall, and is made worse if substantial amounts of low volatility components are present in the fuel. Combustion then occurs as a diffusion flame or pool fire as the fuel evaporates with consequent production of soot [20,21].

For three-way catalyst equipped cars, the particles emitted at the tailpipe are 95% elemental carbon and consist almost entirely of accumulation mode particles (>30 nm) with an average diameter of about 70 nm [22,23]. It has also been noted that much higher levels of particles are generated during acceleration and cold-start operation as compared to steady-state. Therefore, for vehicle emission regulatory purposes steady-state test cycles are not appropriate. However, Aikawa and coworkers show very similar trends in fuel effects on PM emissions for transient and steady-state vehicle driving cycles [13]. Researchers at Honda have shown that for both port fuel injection and DI engines PM emissions are correlated with a particulate matter index (PMI) that can be calculated based on a detailed hydrocarbon analysis (DHA) for a gasoline. PMI is a function of the weight fraction, vapor pressure, and double bond equivalent (DBE) value for each component in the fuel [13,20]. Fuel components with high vapor pressure will evaporate quickly, minimizing diffusive, heterogeneous combustion or avoiding pool fire combustion if piston impingement occurs. The DBE is the number of hydrogen molecules required to saturate the double bonds and open rings present in a fuel molecule. A global survey of 1,445 gasoline samples showed a PMI range of 0.67 to 3.86 with a mean of approximately 1.6. A typical U.S. certification gasoline exhibits a PMI of 1.36 [13].

Ethanol produced from starch is the primary renewable fuel used in SI engines today, and ethanol may have several distinct advantages for application in DISI engines [24,25]. To achieve much larger quantities of biofuel with lower life-cycle greenhouse gas emissions, production must shift to lignocellulosic biomass feedstocks [26], which can be economically converted to ethanol [27]. Nevertheless ethanol is not without its disadvantages, including low volumetric energy content, high water solubility, and potential materials compatibility issues at high blend levels, all of which prevent it from being considered as a drop-in fuel. Thus, a large international research effort is focused on converting lignocellulosic biomass into drop-in fuels, which are conventionally thought to be hydrocarbons. However, biomass typically contains 40 percent by weight (wt%) to 60 wt% oxygen, suggesting that conversion to hydrocarbons will be both technically and economically challenging. Analysis has shown that costs for hydrotreating of pyrolysis oil derived from biomass can exceed $1 per gallon, with particularly high incremental costs for removal of the last increment of oxygen [28,29]. Gasoline boiling range oxygenates from partially upgraded biomass pyrolysis oils or made from biomass by acid or base-catalyzed deconstruction include phenolics, aryl ethers, and furans [30, 31, 32, 33, 34]. Additionally, isobutanol can be produced by fermentation of sugars, including cellulose-derived sugars [35]. Many of these oxygenates have high octane numbers and high energy density [36] and are thus desirable for enabling the deployment of more efficient DISI engines. The study reported here is part of an effort to determine the extent to which biomass oxygenates can function as drop-in fuels. We specifically focus on how the biomass-derived oxygenates ethanol, isobutanol, 2,5-dimethylfuran (DMF), anisole, 4-methylanisole (4-MA), 2,4-xylenol, and 2-phenylethanol (2-PE) impact fuel properties, as well as knock-limited spark advance and PM emissions from a single cylinder DISI engine.

METHODS

Fuels and Fuel Property Measurements

The base gasoline was obtained from a local supplier, and oxygenates were obtained as reagent grade chemicals. p-Xylene (1,4-dimethylbenzene) and p-cymene (1-methyl, 4-isopropylbenzene) were used to increase the base gasoline RON and PMI without adding oxygen. Blends were prepared volumetrically at room temperature, and the blend concentration was confirmed by an in-house gas chromatography method.

DHA was performed by ASTM method D6729. Our implementation of this method via gas chromatography has been previously reported [37]. Once the components were identified and quantified by gas chromatograph, an Excel spreadsheet containing each component name and the percent by weight present was generated. Because a few hundred components were present, we eliminated those present at less than 0.05 wt%, which resulted in less than a 5% total reduction in sample. Heat of vaporization (HoV) was calculated from the DHA as previously described [37].

The actual blend concentration of ethanol was determined by ASTM method D5501. Ethanol blends are designated by Exx, representing the nominal volumetric ethanol concentration. Other oxygenates were measured by an in-house two-dimensional heart-cutting gas chromatography method that has been previously described [36].

PMI was calculated from the DHA as in Aikawa et al. [13]

$$PMI = \sum_{i=1}^{n} \left[\frac{(DBE_i + 1)}{VP(443K)_i} \times Wt_i \right] \quad (2)$$

where the double bond equivalent (DBE) of the individual compound is defined as:

$$DBE = (2C + 2 - H)/2 \quad (3)$$

Wt_i is the weight percent of each component, and VP is the vapor pressure at 443K. Vapor pressures at 443 K were estimated following the Lee and Kesler method [38].

$$P^{sat} = P_r^{sat} * P_c \quad (4)$$

$$lnP_r^{sat} = (lnP_r^{sat})^{(0)} + \omega(lnP_r^{sat})^{(1)} \quad (5)$$

$$(lnP_r^{sat})^{(0)} = 5.92714 - \frac{6.09648}{T_r} - 1.28862\, lnT_r + 0.169347\, T_r^6 \quad (6)$$

$$(lnP_r^{sat})^{(1)} = 15.2518 - \frac{15.6875}{T_r} - 13.4721\, lnT_r + 0.43577\, T_r^6 \quad (7)$$

where P^{sat} is the vapor pressure at a desired temperature, T_r is the reduced temperature (desired temperature/critical temperature), P_c is the critical pressure, and ω is the acentric factor. Critical properties for individual compounds were taken from literature sources [39,40].

Single-Cylinder Engine Experiments

The single-cylinder engine specifications are shown in Table 1. This engine was developed from a 2009 model year GM Ecotec 2.0 L LNF-series engine, with a wall-guided DI combustion system. The dynamometer, engine control, air handling, fuel supply, and combustion analysis systems have all been previously described [23]. A standard procedure for purging the fuel system and running the engine at a high power for a set period of time was performed before testing each new fuel.

Table 1. Single-cylinder engine specifications.

Displacement (L)	0.5
Bore (mm)	86.0
Stroke (mm)	86.0
Connecting rod length (mm)	145.5
Compression ratio	9.2
Number of valves	4
Combustion System	Wall-guided Direct Injection

For spark timing sweep experiments, a relatively low engine speed was used because longer combustion duration increases exposure of the unburned end-gas to heat and pressure making the engine more sensitive to autoignition and knock. Experimental conditions were a nominal load of 925 kPa net mean effective pressure (NMEP), 1,500 rpm, and intake air temperature of 35°C (measured at the intake port). The load and intake air temperature were selected to ensure the engine could operate on the 88 RON hydrocarbon base gasoline. Cam phasing, fuel pressure, and start of injection were based on GM calibration data for this speed and load (see Table 2). Spark timing was initially set to 10 crank angle degrees (CAD) before top dead center (BTDC), fuel and air flows were adjusted slightly lean (0.3% - 0.5% oxygen in the exhaust gas). For each spark sweep the fuel and air flows were held constant after achieving the nominal 925 kPa NMEP load at 10° BTDC spark advance. Absolute fueling rates were unique to each blend because of energy and gravimetric density differences. Spark was then advanced in one or two degree increments. The engine output (load) increased up to minimum advance for best torque (MBT) because combustion phasing becomes optimal there.

Maximum pressure rise rate (MPRR) was used as a real-time measure of impending or actual knock, and spark timing was advanced until any cycle during the 100-cycle data collection period exceeded 1,100 kPa/CAD (the programmed limit triggering automatic spark retard). It should be noted that this MPRR limit turned out to be too aggressive (strong knock) and is not to be mistaken as a recommended practice. Integrated knock, or knock-integral (KI) was calculated by first filtering the in-cylinder pressure signal using a second-order Butterworth band-pass filter (5 - 15 kHz band), then rectifying the filtered signal [41]. A knock window was selected starting at 5° after top dead center and lasting for 30°. A reference window was selected starting at 210° BTDC and 30° duration. The filtered, rectified signal was then integrated separately over both the knock and reference windows. The KI value is defined by:

$$KI \quad \int_{Knock} / \int_{Reference} - Threshold \quad (8)$$

The threshold value chosen for this study was 0.5 KI units.

Table 2. Engine operating parameters.

Engine Speed/Load (rpm/kPa)	**2,500/ 1,300**	**2,000/ 300**	**1,500/ 600**	**1,500/ 925 @ start of spark sweep**
Intake Press (bar abs)	1.15	0.46	0.70	0.86
Intake Temp (°C)	35	35	35	35
Fuel Rail Pressure (bar)	68	35	68	68
Start of Injection (°BTDC)	300	265	270	290
Spark Timing (°BTDC)	10	28	28	10. sweep starting point
Intake Cam Phasing (CAD)[a]	30	30	35	40
Exhaust Cam Phasing (CAD)[b]	20	25	30	35
Coolant / Oil Temp (°C)	85 / 90			
Equivalence Ratio	0.98			

[a]CAD advanced from full retard. [b]CAD retarded from full advance.

Three separate engine speed and load operating points were used to evaluate fuel effects on PM-mass and PN emissions. These were 2,500 rpm-1,300 kPa NMEP; 2,000 rpm-300 kPa NMEP; and 1,500 rpm-600 kPa NMEP. Engine operating parameters for the PM experiments are shown in Table 2. The engine was operated slightly lean to ensure repeatable PM measurements, i.e., stoichiometric operation produced large PM measurement variations from minor air-fuel ratio instabilities. PM-mass, PN, and engine data were recorded for 1 minute at 1 Hz and then averaged. Each engine operating point was run several times in a randomized order across several days for each fuel.

The PN emission measurement system consists of a Dekati FPS-4000 two-stage exhaust sample dilution system upstream of a Dekati Thermodenuder feeding the diluted sample to a TSI Fast Mobility Particle Sizer (FMPS) model 3091. The Dekati dilution system uses a primary perforated wall flow type dilutor with dilution air that is temperature controlled (set to 150°C). The secondary stage of the dilutor is an ejector dilutor that uses room temperature dilution air and acts as the main driving force for the diluted exhaust sample flow. The overall dilution ratio was set to between 25:1 and 30:1 for all of the testing in this study. The Dekati Thermodenuder operating temperature was 275°C. The TSI FMPS measures PN distribution for particle diameters between 5.6 to 560 nm with a 32-channel resolution. The Thermodenuder is intended to remove all volatile compounds, so that the resulting FMPS measurements are theoretically on a strictly elemental carbon emissions basis. This sample processing was done because studies have shown that DISI engine vehicles equipped with a three-way exhaust catalyst emit primarily elemental carbon PM [22]. Separately, an AVL Micro-Soot Sensor (MSS) is connected to the raw engine exhaust and measures real-time PM-mass. The MSS includes contains its own built in dilution system, which was nominally set to an 8:1 ratio.

RESULTS AND DISCUSSION

Fuel Properties

The properties of the gasoline base fuel have been reported previously [37], but are reproduced here for completeness. Compound classes and other properties of the base gasoline derived from the DHA are shown in Table 3. The base gasoline was a sub-octane blendstock for oxygenate blending intended for summertime use in an ozone non-attainment area. Particle emissions and PMI will be affected by aromatic and olefin content, and these values are in the middle range for U.S. gasoline [42].

Net heating values and boiling points for the oxygenates examined are shown in Figure 1, and other properties are listed in Table 4. The high boiling points of 2-PE and 2,4-xylenol relative to the gasoline end point limit of 225°C are notable, as are the high volumetric energy densities of several of the oxygenates relative to conventional gasoline. All exhibit high octane number. The blending RON and MON values are reported in Table 4 because some of the compounds' volatilities are too low to have their RON and MON measured directly. However, it must be noted that blending RON and blending MON cannot be considered absolute values because they depend on the chemistry of the base fuel and blending level. Furthermore, any errors in the octane numbers and concentration measurements are amplified by the equation for calculating these blending octane numbers, especially at low blending levels. For example, at the 20 vol% blend level, blending octane number can be computed as:

$$Blending\ Octane\ Number = [(Blend\ ON) - (0.8) * (Base\ Fuel\ ON)] / 0.2 \quad (9)$$

In this example, division by the volume fraction 0.2 results in a fivefold increase in error of the measured quantities in the resulting blending octane number.

Table 3. PIANO analysis and other properties of the base gasoline.

Paraffins	D6729	vol%	11.5
Isoparaffins	D6729	vol%	47.9
Aromatics	D6729	vol%	23.7
Naphthenes	D6729	vol%	7.8
Olefins	D6729	vol%	8.4
Average MW	D6729	g/mol	95.9
Carbon	D6729	wt%	86.1
Hydrogen	D6729	wt%	13.9
Density at 15°C	D4052	g/ml	0.7374
Dry vapor pressure equivalent (Reid vapor pressure equivalent)	D5191	Psi	6.86
Distillation T_{10}	D86	°C	61
Distillation T_{50}	D86	°C	98
Distillation T_{90}	D86	°C	154
Final Boiling Point	D86	°C	198

PIANO – paraffins, isoparaffins, aromatics, naphthenes, and olefins

Ethanol and isobutanol have high vapor pressure at 443 K and a DBE value of zero, so do not cause PMI to increase. DMF has a relatively high vapor pressure but a DBE of 3 and would be expected to moderately increase PMI. Anisole, 4-MA, 2,4-xylenol, and 2-PE have much lower vapor pressures at 443 K and have DBEs of 4, causing PMI to increase. These expectations are met as shown in Table 5, which presents properties of the gasoline blendstock-oxygenate blends. Blends were also prepared with p-xylene (20 vol%) and p-cymene (20 vol%) to demonstrate the impacts of increasing aromatic content without fuel oxygen. The Sunoco GTX demonstrates that high aromatic content (45.5 vol%) can be offset by high vapor pressure at 443 K (note low T_{90}) resulting in a low PMI fuel. Distillation curves of selected fuels are shown in Figure 2. Blending with 20 vol% 2-PE causes the gasoline to fail the maximum limit for T_{90} and nearly fail for T_{50}. The 10 vol% 2,4-xylenol blend nearly fails T_{90}, and the 21% 4-MA blend nearly fails T_{50}. The relatively high boiling point of these oxygenates significantly limits levels that can be blended into ASTM D4814-compliant gasoline.

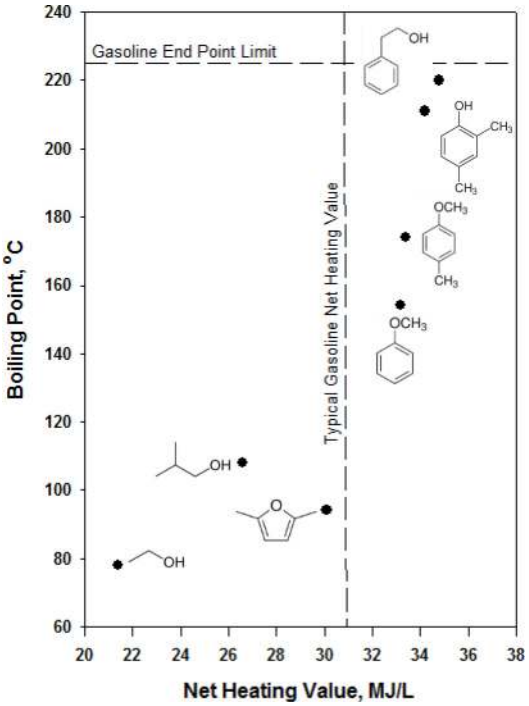

Figure 1. Boiling point and net heating value for the biomass-derived oxygenates.

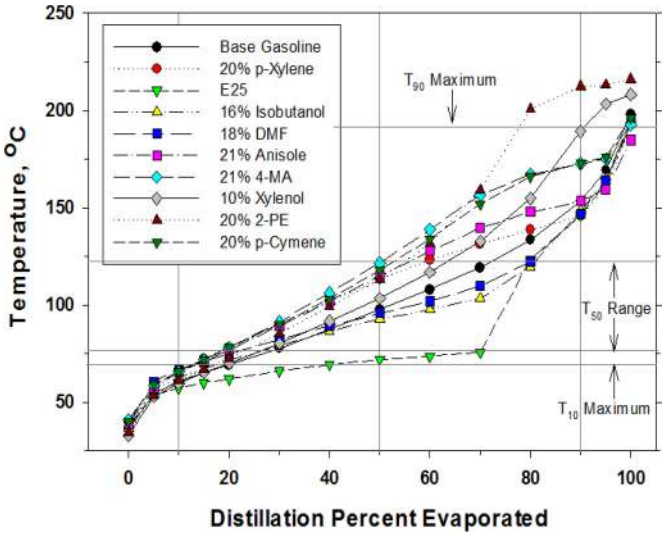

Figure 2. Distillation curves by ASTM method D86 for gasoline oxygenate blends. Limits shown are for Class AA or Class A volatility class gasoline.

Table 4. Properties of biomass-derived oxygenates.

Compound	Structure	Blending RON / MON[a]	HoV (kJ/kg)[43]	Net Heating Value (MJ/L)	Vapor Pressure @ 443 K (kPa)	Boiling Point (°C)[44,46]	DBE
Ethanol		131 / 103[b]	921	21.4[44]	1,550	78	0
Isobutanol	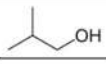	116 / 88	634	26.6[44]	596	108	0
2,5-Dimethylfuran (DMF)		141 / 104	379	30.1[44]	538	94	3
Anisole		124 / 102	419	33.2[c]	154	154	4
4-Methylanisole (4-MA)	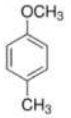	129 / 99	377	33.4[c]	87.7	174	4
2,4-Xylenol	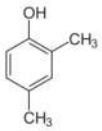	197 / 159	530	34.2[c]	30.3	211	4
2-Phenylethanol (2-PE)		132 / 99	561	34.8[c]	21.5	220	4
p-Xylene	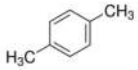	124 / 97	399	35.4[45]	218	138	4
p-Cymene	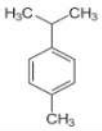	124 / 101	365	35.5[45]	84.5	177	4

[a]For blends in this work. [b]For E25. [c]This work.

Table 5. Properties of the gasoline blendstock, its oxygenate blends and control fuels.

Fuel Blend	Blend Level (wt% / vol%)	Oxygen (wt%)	RON / MON	HoV at 25°C (kJ/kg)	Net Heating Value (MJ/L)	T_{50} / T_{90} (°C)	PMI
Base Fuel	--	0	87.9 / 81.9	352.8	32.1	98 / 154	1.07
Ethanol (E10)	9.9 / 9.3	3.5	93.0 / 84.1	415.5	30.8	86 / 152	0.97
Ethanol (E25)	27.6 / 26.0	9.6	99.1 / 87.4	527.3	29.1	72 / 146	0.80
Ethanol (E50)	49.2 / 47.1	17.1	102.6 / 88.7	662.3	26.8	75 / 81	0.58
Isobutanol	16.7 / 15.5	3.6	92.3 / 82.8	398.4	31.0	93 / 149	0.92
2,5-Dimethylfuran (DMF)	20.1 / 17.0	3.4	96.9 / 85.6	371.4	31.6	96 / 147	1.01
Anisole	24.7 / 19.6	3.7	95.0 / 85.8	371.8	32.3	115 / 154	1.61
4-Methylanisole (4-MA)	26.3 / 21.4	3.5	96.7 / 86.5	360.6	32.4	122 / 173	2.20
2,4-Xylenol	13.3 / 10.0	1.8	98.8 / 89.6	371.1	32.3	103 / 189	3.13
2-Phenylethanol (2-PE)	22.3 / 17.2	2.9	95.4 / 86.0	399.5	32.5	113 / 212	6.03
p-Xylene	25.5 / 20.0	0	95.1 / 84.9	363.2	32.6	113 / 146	1.36
p-Cymene	23.3 / 20.0	0	95.3 / 85.7	347.8	32.7	118 / 173	2.19
Sunoco GTX	--	0	103 / 93	364.2	32.6	104 / 108	0.70

Single-Cylinder Engine Results

Knock Limited Spark Advance

KI averages of 100 engine cycles versus spark advance for all fuels tested are shown in Figure 3. Inspection of the cylinder pressure curves for knock, led to selecting the knock-limited spark advance (KLSA) level as occurring at KI = 10. This was correlated with MPRR values of 500 ±30 kPa/CAD, and above this level the engine was experiencing knock. Among the non-oxygenated control fuels, the 87.9 RON base fuel exhibited a KLSA of 14° BTDC, the p-xylene blend (RON 95.1) had a KLSA of 19° BTDC, the p-cymene (RON 95.3) blend had a KLSA of 19.5° BTDC, while the 103 RON Sunoco GTX was far removed from knock at this operating condition. It is worth noting that some fuels exhibited different slopes as KI rapidly increased, and in particular the slope for the E25 blend was lower, and remained lower crossing the KLSA level than did slopes for the other fuels.

Figure 4 plots KLSA versus RON for all fuels studied except for E50 and Sunoco GTX, which were not knock limited in this engine at the test conditions. In the octane index proposed by Kalghatgi (Equation 1), RON is the case where K = 0 and linear regression produced a correlation coefficient, $R^2 = 0.870$. Table 6 summarizes correlation coefficients for KLSA against a series of OIs with K ranging from 1 to -0.25. The maximum correlation was when K = 0.25. From this analysis it appears that K for this engine and operating condition approximates the RON method. This is reasonable given the low intake air pressure and temperature, spark timing near minimum advance for best torque (MBT), and modest compression ratio [6,47].

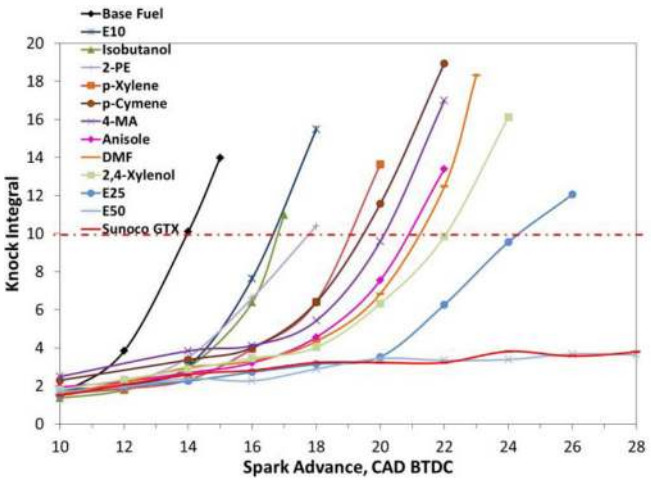

Figure 3. KI vs. spark advance for all fuels at 1,500 rpm, 925 - 990 kPa NMEP. The dashed red line indicates the KLSA level, above which the engine was knocking.

Spark sweep results for the control fuels and non-ethanol oxygenate blends that had distillation T_{90} less than or equal to that for the base fuel are shown in Figure 5. The low octane base gasoline exhibited a KLSA of 14° BTDC, and triplicate spark sweeps revealed a maximum NMEP standard deviation of 3.6 kPa at 12° BTDC, while the average standard deviation was less than 2 kPa. The MBT spark advance for DMF and anisole blends was 20° BTDC, as indicated by the peak NMEP. The p-xylene blend had strong knock (at the maximum pressure rise rate limit) at 20° BTDC in spite of having 95.1 RON, similar to the anisole blend.

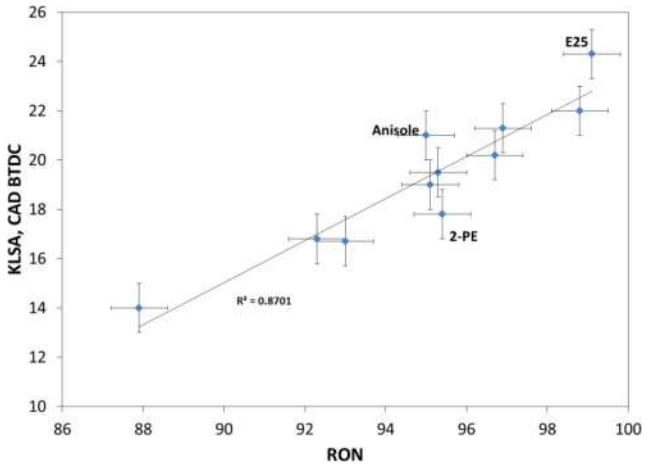

Figure 4. KLSA vs. RON for fuels with RON less than 100. X-axis error bars are ±0.7 RON units (D2699 stated reproducibility for the RON range 90-100). Y-axis error bars are ±1.0 CAD based on results of repeated measurements.

Table 6. Correlation coefficients from linear regression of KLSA vs. OIs.

K	R^2 for KLSA vs. OI, all fuels < 100 RON
1.0	0.756
0.5	0.864
0.25	**0.874**
0.1	0.873
0.0	0.870
-0.1	0.866
-0.25	0.859

Figure 6 shows the spark sweep curves for the oxygenate blends that had T_{90} distillation points greater than the base gasoline's. Given that 2,4-xylenol was blended at roughly half the concentration as the other non-ethanol oxygenates (see Table 5), this blend's high RON and KLSA performance are noteworthy. In contrast, the 2-PE blend underperformed relative to its measured RON producing a KLSA of 18° BTDC, while the nominally equivalent RON control fuels p-cymene and p-xylene (shown in Figure 5) achieved KLSAs of 19.5° BTDC and 19° BTDC, respectively. 2-PE's underperformance was also indicated in Figure 4, and the explanation is probably related to the profoundly negative affect 2-PE had on the D86 distillation curve (see Figure 2). The upper 30% of this curve is significantly elevated in temperature and this was the only fuel blend studied where T_{90} exceeded the ASTM D-4814 upper limit of 190°C. We speculate that 2-PE (and perhaps other low vapor pressure compounds) was not fully vaporizing in the engine cylinder, leading to fuel spray impingement on the piston and cylinder wall and consequently to diffusion combustion. Thus, it seems plausible that low vapor pressure and impingement led to a depletion of 2-PE in the end gas which reduced the fuel's knock resistance. In the ASTM method for RON, fuel is mixed with higher temperature air (52°C) in a carburetor upstream of the intake valve and therefore has longer contact with warmer air and even hotter engine surfaces enabling more of the fuel to evaporate than in a DISI engine. These differences may explain the observed variance between 2-PE's KLSA measured in the DISI engine and the measured RON.

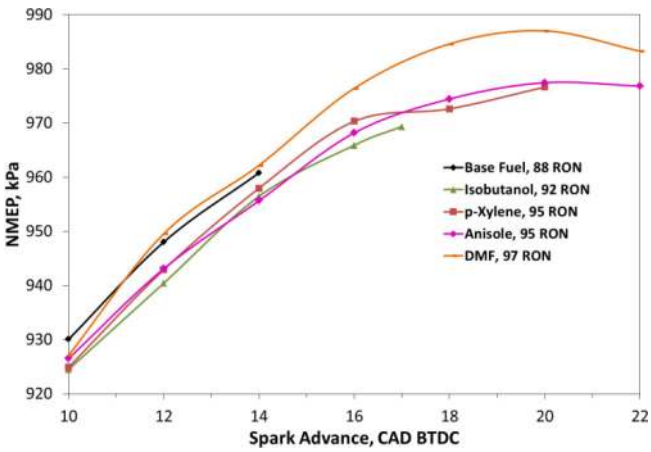

Figure 5. 1,500 rpm NMEP vs. spark advance to ~KLSA for control fuels, isobutanol, DMF, and anisole blends. Note that actual KLSAs (KI = 10) were 19° BTDC for p-xylene, 21° BTDC for anisole, and 21.3° BTDC for DMF.

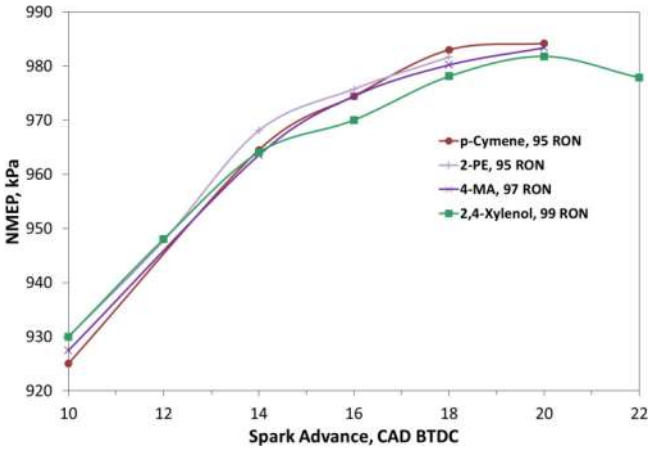

Figure 6. 1,500 rpm NMEP vs. spark advance to ~KLSA for oxygenate blends with T_{90} greater than the base fuel's. KLSA for p-cymene was 19.5° BTDC.

In addition to fuel autoignition chemistry, knock resistance for DISI engines may be enhanced by fuel-air charge cooling as the fuel evaporates, which reduces the end-gas temperature. This is an important effect in DISI engines regardless of fuel type. The HoV of gasoline hydrocarbons is 350 to 400 kJ/kg at 25°C while that of ethanol is 920 kJ/kg [37,48]. As shown in Table 4, several of the biomass-derived oxygenates also exhibit HoV significantly higher than that of gasoline boiling range hydrocarbons and thus potentially have knock resistance over and above that provided by their high RON. However, as shown in Table 5, in most cases the impact on HoV is relatively small, the exceptions being the E25 and E50 blends. Based on their similar RONs of ~99, it would be expected that the 2,4-xylenol and E25 blends would have the same KLSAs. However, as Figure 7 shows, E25 was able to tolerate additional spark advance (24.3° BTDC) compared to the 2,4-xylenol blend (22° BTDC) before reaching KLSA. The HoV for the E25 blend was calculated to be 527 kJ/kg and that for the 2,4-xylenol blend was 371 kJ/kg (see Table 5), the latter being close to the base gasoline's. Thus, additional charge cooling from ethanol in

the E25 blend may explain the enhanced KLSA performance of this fuel. Another factor may have been reduced knock resistance from 2,4-xylenol for the same reasons postulated for 2-PE, given the similarly high boiling point of this molecule.

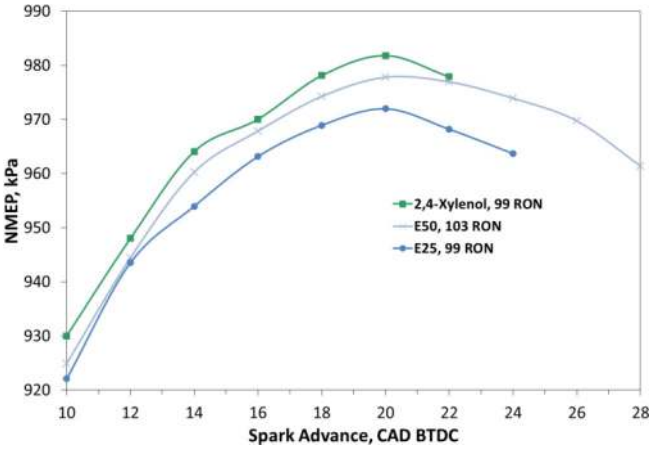

Figure 7. 1,500 rpm NMEP vs. spark advance to ~KLSA for 2,4-xylenol, E25, and E50 blends. E25 KLSA was 24.3° BTDC; E50 was not knock-limited.

Particle Emissions

Figure 8 shows the PM-mass results for all three speed-load conditions. The E10 fuel data were anomalous and discarded from the particle emission results because of suspected fuel cross-contamination from the engine lube oil. At the lowest load condition (bottom panel), PM-mass concentrations are very low and it is difficult to discern differences between fuels. PM-mass emission levels at this condition may be below or only slightly above the detection limit of our measurement system for most fuels. Nevertheless, the PM-mass emissions from the p-xylene control fuel and 4-MA were clearly higher than from the base gasoline, as expected from their higher PMIs. More differentiation is apparent at the intermediate load (center panel), but at 2,500 rpm-1,300 kPa NMEP PM-mass emissions are 2 to 10 times higher. Here, fuel effects are evident with significantly higher (statistical p-value < 0.01) emissions observed for fuels spiked with aromatic/low vapor pressure components (components with high PMI) relative to the base gasoline. The fuel effects on engine exhaust total PN concentration can be seen in Figure 9 for the 2,500 rpm-1,300 kPa NMEP condition. The error bars represent the 95% confidence interval. As was the case for the PM-mass results, PN emissions showed much higher emission levels than from the lower load points, and generally revealed the expected trends of higher emissions ($p < 0.01$) with higher PMI fuels relative to the base gasoline.

Particle size distribution plots are displayed on a log-log chart. The x-axis of particle diameter is fairly straightforward but the y-axis of PN dN/dlogDp is not. The FMPS measures particles in the size ranges from 5.6 to 560 nm. This range is split into 32 channels or bins. The smallest diameter size bin counts particles with a nominal or midpoint size of 6.04 nm and the bin boundaries are roughly 0.5 nm above and below that. The largest diameter size bin counts particles with a nominal midpoint diameter of 523.3 nm and the bin ranges roughly 40 nm above and below that. The bin for the largest diameter particles is roughly 80 times wider than the smallest bin.

Because we are reporting the number of particles that fall within each bin, the result would appear that there are 80 times more particles in the largest bin than in the smallest bin because it is 80 times wider. To overcome this problem, the particle number is normalized by the width of its respective bin. The particle count is roughly divided by 1 for the smallest bin and 80 for the largest bin so that it shows a more representative distribution of particle count across the size range for each channel.

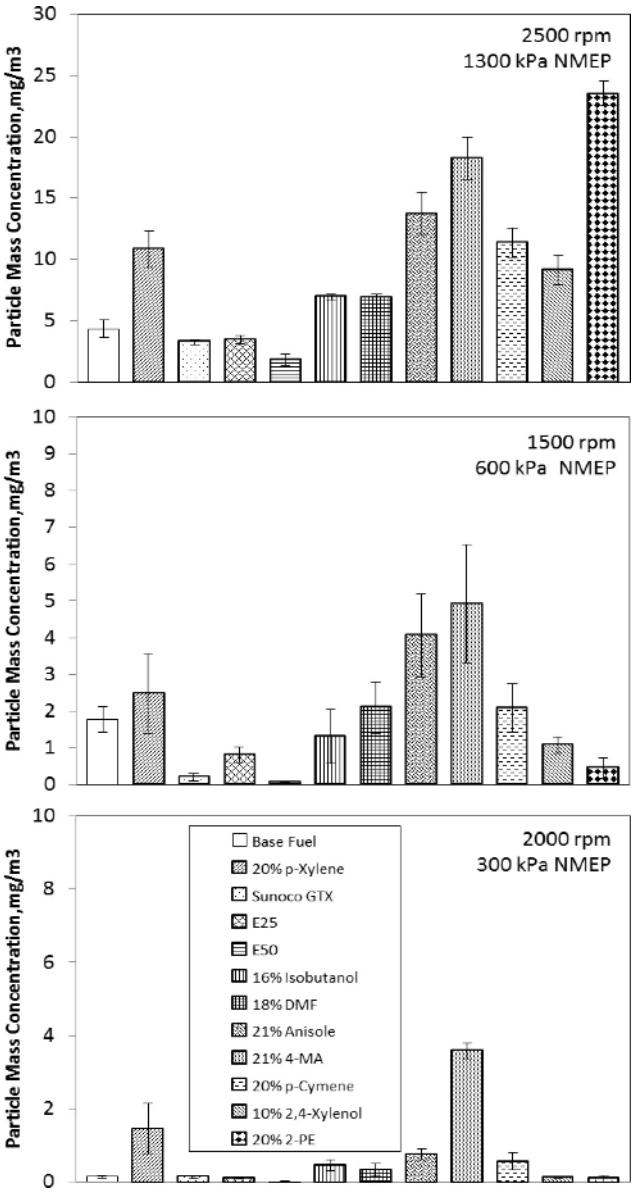

Figure 8. PM-mass concentration (error bars are 95% confidence interval).

Examination of the data in Figure 10 for operation at 2,500 rpm-1,300 kPa shows very similar size distribution for all fuels with a nucleation mode centered at about 10 nm and accumulation mode centered at 60 to 70 nm. The data are generally consistent with the total PN results; for example, the E50 blend showed the lowest PM-mass and total PN emissions, consistent with the much lower level of particles in the accumulation mode. The correlation between particle number and particle mass concentrations at 2,500 rpm-1,300

kPa is shown in Figure 11. The strong correlation is expected for particles that are predominantly elemental carbon, accumulation-mode particles [22,23].

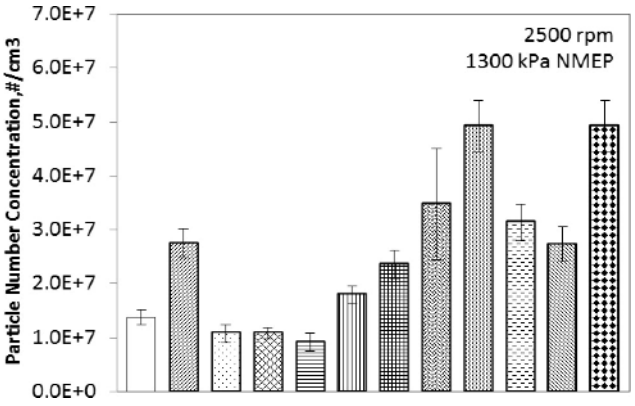

Figure 9. PN concentrations at the high speed, high low condition (error bars are 95% confidence interval, legend same as Figure 8).

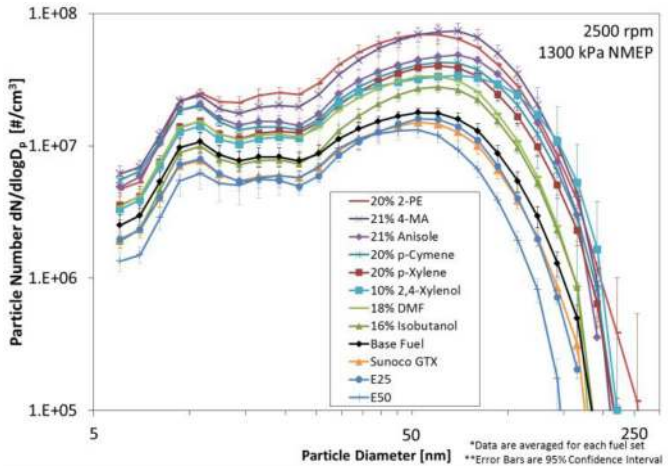

Figure 10. PN size distribution for 2,500 rpm-1,300 kPa NMEP (log-log plot, error bars are 95% confidence interval).

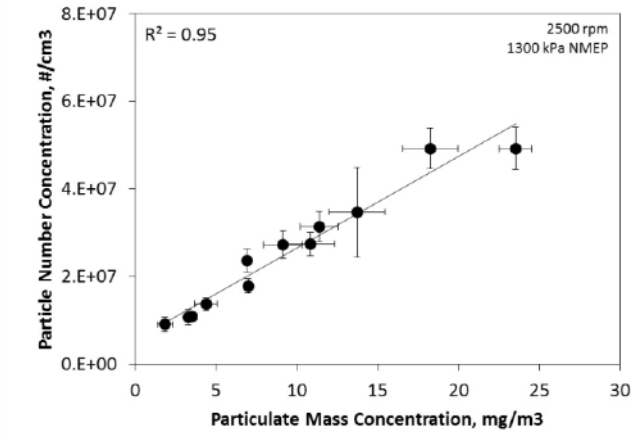

Figure 11. Correlation between PM-mass and PN concentrations for all fuels at 2,500 rpm-1,300 kPa NMEP.

Figure 12 shows the correlation between PM-mass concentration and PMI, while Figure 13 shows the correlation between PN concentration and PMI. For most fuels there was good correspondence of PM-mass and PN emissions with PMI; however, in both cases results for 2,4-xylenol and 2-PE were not included in the linear regression as they fall significantly away from the trend for the other fuels, emitting less PM than predicted by PMI. The lowest PM-mass and PN emissions were observed for E50, which also had the lowest PMI (0.58) and the highest fuel oxygen content. E25 and Sunoco GTX each have PMIs between those for the base gasoline and E50, and their PM-mass emissions fall in between, as expected.

Isobutanol and DMF slightly increased PM-mass and PN over the base gasoline at 2,500 rpm-1,300 kPa despite having slightly lower PMIs (0.92 and 1.0, respectively), which may simply reflect small measurement errors in both PM emissions and in the parameters used to estimate PMI. However, higher isobutylene emissions have been measured from an isobutanol-gasoline fueled vehicle, so it is possible that in-cylinder isobutylene formation contributed to molecular weight growth and therefore to PM [49]. In the case of DMF, once the furan ring opens, reactive olefins are likely produced, which similarly may lead to molecular weight growth.

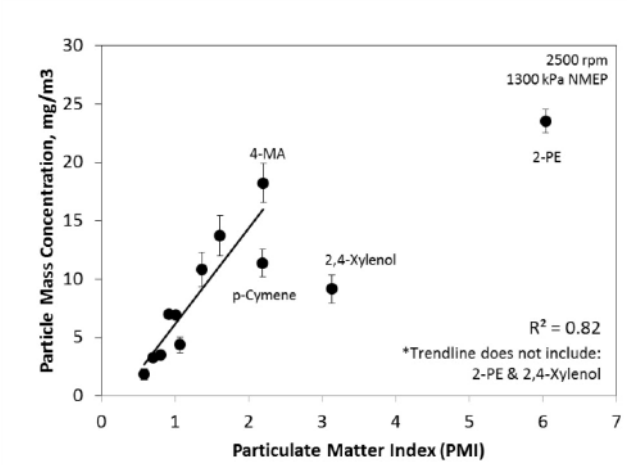

Figure 12. PMI correlation with PM-mass from 2,500 rpm-1,300 kPa NMEP.

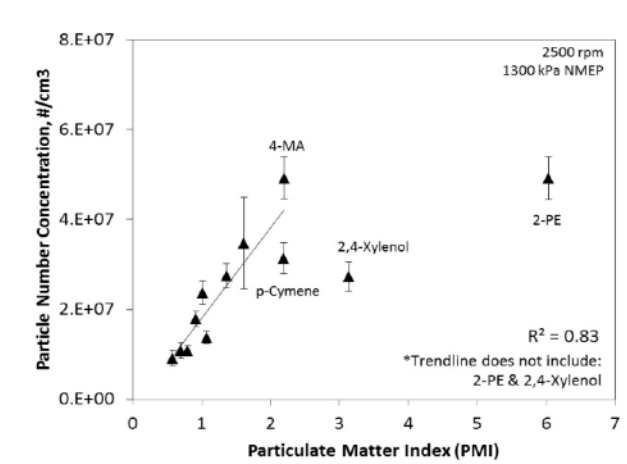

Figure 13. PMI correlation with total PN concentration from 2,500 rpm-1,300 kPa NMEP.

The difference in results between 4-MA and p-cymene, which have the same PMIs, was also unexpected because they have nearly identical boiling points and vapor pressures (at 443 K), and produced similar knock-limited performance (see Figure 6). Yet 4-MA produced higher PM-mass and PN emissions. Studies of anisole pyrolysis show that its decomposition proceeds through homolysis of the O-CH_3 bond to phenoxy radical. This further decomposes to cyclopentadienyl radical, which can couple to form naphthalene initiating chain or molecular weight growth [50,51]. No similarly facile route to phenoxy radical exists for aromatic hydrocarbons, which must add oxygen to the ring. Taken as a whole, these observations for isobutanol, DMF, and 4-MA suggest that combustion effects may exist for blending some oxygenates with gasoline that are not captured by the current PMI relationship (Equation 2).

In comparing results for both PM-mass and PN to the PMI predicted trend, both 2-PE (PMI = 6.0) and 2,4-xylenol (PMI = 3.1) are not as high as expected. It is notable that both of these blend components boil above 200°C, significantly increase the blend T_{90}, and have the lowest vapor pressures at 443 K of all of the oxygenates tested. The T_{90} for the 2-PE blend is well above the allowable T_{90} limit for gasoline in ASTM D4814. As discussed above, 2-PE underperformed for knock resistance; we speculated that this was caused by 2-PE failing to fully evaporate, therefore being depleted in the end gas. Incomplete evaporation may also be the reason for the lower than expected PM-mass and PN emissions from 2-PE and 2,4-xylenol. The T_{90} limit for gasoline exists, in part, to protect engines from accumulation of unburned fuel in the lubricant. While it is anecdotal, we observed by smell that the engine lube oil retained the four lowest vapor pressure fuels, each of which has a distinctive odor, supporting the idea that these blend components do not fully evaporate. This idea further is supported by data in Figure 14 that show a strong correlation between total hydrocarbon emissions and PM-mass. If 2-PE and 2,4-xylenol were evaporating but not combusting (therefore also not forming PM), we would expect anomalously high total hydrocarbon (THC) emissions relative to the other fuels. But this was not the case.

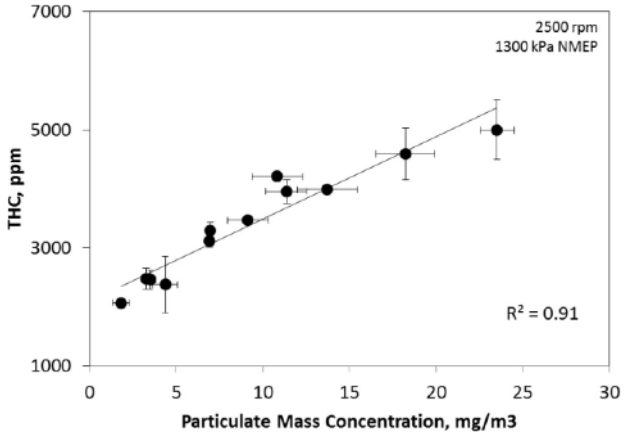

Figure 14. THC correlation with PM-mass concentration for all fuels at 2,500 rpm-1,300 kPa NMEP.

The difficulty in fully evaporating the high boiling 2-PE and 2,4-xylenol may have been enhanced by engine operating parameters. At 2,500 rpm-1,300 kPa NMEP, the start of injection was 300° BTDC (i.e., 60° after the start of the intake stroke), so the piston was still relatively high in the cylinder and accelerating down while the injector pulse widths were the longest (~3.5 mS) of all test points. Consequently, fuel spray impingement on the piston and/or cylinder wall was possible. This combined with low volatility and low reactivity fuel components may have made their evaporation and combustion difficult.

CONCLUSIONS

Our objective in this work was to determine the effects of a small group of oxygenated molecules, representative of those that could be derived from biomass, on DISI engine knock-resistance and particle emissions. The high octane oxygenates were blended with a sub-octane gasoline blendstock intended for blending with ethanol. Fuel properties of the blends were measured, and a modern DISI engine was used to measure their knock resistance and PM emissions. Two of the oxygenates, 2-PE and 2,4-xylenol, significantly increased the T_{90} distillation temperature in the D86 distillation curve. The 20% 2-PE blend failed the T_{90} limit for gasoline. The high boiling points of these oxygenates will significantly limit their use in gasoline, probably to less than a few vol%.

It was found that RON was a good predictor of knock-limited performance for all fuels tested, consistent with an estimated K value of 0 to 0.25 for the engine operating conditions used in the study. The 2-PE blend underperformed in terms of a lower KLSA than the blended p-xylene and p-cymene control fuels, which had the same RON. We speculate that 2-PE's lower KLSA was associated with its low volatility leading to depletion of 2-PE in the end gas. The E25 blend was found to have a higher KLSA than the 2,4-xylenol blend with the same RON, possibly because of ethanol's enhanced charge cooling in the DISI engine. An additional factor may have been reduced knock resistance of 2,4-xylenol for the same reasons postulated for 2-PE, given the similarly high boiling point of this molecule.

Particle emission effects of the fuels were revealed at the highest load condition employed of 2,500 rpm and 1,300 kPa NMEP. Isobutanol produced a small increase in both PM-mass and PN emissions, similar to that from DMF. This was inconsistent with isobutanol's relatively low boiling point, high vapor pressure, and lack of unsaturated structures. Anisole, 4-MA, 2-PE, and 2,4-xylenol caused a significant increase in both PM-mass and PN emissions (by factors ranging from 2 to 5) relative to the base gasoline. Thus, any effect of their oxygen atom to reduce PM by increasing local air-fuel ratio is outweighed by their low vapor pressure and high DBE values. The boiling point of 2-PE (220°C) and 2,4-xylenol (211°C) and their very low vapor pressures may have significantly altered performance properties that are critical to DISI engine performance. Yet PM-mass and PN emissions were lower than would be predicted by correlation with PMI, suggesting abnormal or incomplete combustion. Consistent with the knock resistance results, these high boiling blend components likely did not fully evaporate and were swept into the lube oil, making them unavailable for particle formation.

Results for several of the oxygenates suggest that the current equation for calculating PMI does not include factors capturing all chemical effects of oxygenates blended into gasoline on PM emissions. Additional investigation of this is warranted.

REFERENCES

1. Intergovernmental Panel on Climate Change, *Fifth Assessment Report: Climate Change 2014: Mitigation of Climate Change*, http://www.ipcc.ch/report/ar5/wg3/, accessed September 7, 2014.
2. Lane, J., "Biofuels Mandates Around the World: 2014," *Biofuels Digest*, December 31, 2013. http://www.biofuelsdigest.com/bdigest/2013/12/31/biofuels-mandates-around-the-world-2014/
3. Energy Independence and Security Act of 2007, Public Law 110-140, Title II, Subtitle A, Sec. 202. Renewable Fuel Standard, December 19, 2007.
4. U.S. Environmental Protection Agency, *EPA and NHTSA Set Standards to Reduce Greenhouse Gases and Improve Fuel Economy for Model Years 2017-2025 Cars and Light Trucks*, EPA-420-F-12-051, August 2012.
5. Fraser, N., Blaxill, H., Lumsden, G., and Bassett, M., "Challenges for Increased Efficiency through Gasoline Engine Downsizing," *SAE Int. J. Engines* 2(1):991-1008, 2009, doi:10.4271/2009-01-1053.
6. Mittal, V. and Heywood, J., "The Shift in Relevance of Fuel RON and MON to Knock Onset in Modern SI Engines Over the Last 70 Years," *SAE Int. J. Engines* 2(2):1-10, 2010, doi:10.4271/2009-01-2622.
7. Stein, R., Polovina, D., Roth, K., Foster, M., et al., "Effect of Heat of Vaporization, Chemical Octane, and Sensitivity on Knock Limit for Ethanol-Gasoline Blends," *SAE Int. J. Fuels Lubr.* 5(2):823-843, 2012, doi:10.4271/2012-01-1277.
8. Kalghatgi, G., "Fuel Anti-Knock Quality- Part II. Vehicle Studies - How Relevant is Motor Octane Number (MON) in Modern Engines?," SAE Technical Paper 2001-01-3585, 2001, doi:10.4271/2001-01-3585.
9. Mittal, V., Heywood, J., and Green, W., "The Underlying Physics and Chemistry behind Fuel Sensitivity," *SAE Int. J. Fuels Lubr.* 3(1):256-265, 2010, doi:10.4271/2010-01-0617.
10. Mittal, V. and Heywood, J., "The Relevance of Fuel RON and MON to Knock Onset in Modern SI Engines," SAE Technical Paper 2008-01-2414, 2008, doi:10.4271/2008-01-2414.
11. Price, P., Stone, R., Collier, T., and Davies, M., "Particulate Matter and Hydrocarbon Emissions Measurements: Comparing First and Second Generation DISI with PFI in Single Cylinder Optical Engines," SAE Technical Paper 2006-01-1263, 2006, doi:10.4271/2006-01-1263.
12. Aakko, P. and Nylund, N., "Particle Emissions at Moderate and Cold Temperatures Using Different Fuels," SAE Technical Paper 2003-01-3285, 2003, doi:10.4271/2003-01-3285.
13. Aikawa, K., Sakurai, T., and Jetter, J., "Development of a Predictive Model for Gasoline Vehicle Particulate Matter Emissions," *SAE Int. J. Fuels Lubr.* 3(2):610-622, 2010, doi:10.4271/2010-01-2115.
14. State of California Air Resources Board, *Preliminary Discussion Paper-Proposed Amendments to California's Low-Emission Vehicle Regulations-Particulate Matter Mass, Ultrafine Solid Particle Number, and Black Carbon Emissions*; State of California Air Resources Board: Sacramento, CA, 2010; http://www.arb.ca.gov/msprog/levprog/leviii/meetings/051810/pm_disc_paper-v6.pdf.
15. U.S. Environmental Protection Agency, *Integrated Science Assessment for Particulate Matter*, Final Report EPA/600/R-08/139F, 2009.
16. Ramanathan, V., and Carmichael, G., "Global and Regional Climate Changes due to Black Carbon," *Nature Geoscience* 1:221-227, 2008. http://www.nature.com/ngeo/journal/v1/n4/full/ngeo156.html
17. California Air Resources Board, *Attachment A-3, "California 2015 and Subsequent Model Criteria Pollutant Exhaust Emission Standards and Test Procedures and 2017 and Subsequent Model Greenhouse Gas Exhaust Emission Standards and Test Procedures for Passenger Cars, Light-Duty Trucks, and Medium-Duty Vehicles*, Amendments to the Low-Emission Vehicle Program - LEV III; California Air Resources Board, 2012. http://www.arb.ca.gov/msprog/levprog/leviii/leviii.htm.
18. European Union Regulation 459/2012, "Commission Regulation (EU) No. 459/2012 of 29 May 2012, Amending Regulation (EC) No. 715/2007 of the European Parliament and of the Council and Commission Regulation (EC) No 692/2008 as regards Emissions from Light Passenger and Commercial Vehicles (Euro VI)," *Off. J. Eur. Union* 2012, L 142, 16-24.
19. U.S. Environmental Protection Agency, *EPA Sets Tier 3 Tailpipe and Evaporative Emission and Vehicle Fuel Standards*, EPA-420-F-14-008, March 2014.
20. Aikawa, K., and Jetter, J.J., "Impact of Gasoline Composition on Particulate Matter Emissions from a Direct-Injection Engine: Applicability of Particulate Matter Index," *Int. J. Eng. Res.* 15(3):298-306, 2013. doi: 10.1177/1468087413481216 http://jer.sagepub.com/content/15/3/298.abstract
21. Fatouraie, M., Wooldridge, M., and Wooldridge, S., "In-Cylinder Particulate Matter and Spray Imaging of Ethanol/ Gasoline Blends in a Direct Injection Spark Ignition Engine," *SAE Int. J. Fuels Lubr.* 6(1):1-10, 2013, doi:10.4271/2013-01-0259.
22. Maricq, M.M., Szente, J.J., and Jahr, K., "The Impact of Ethanol Fuel Blends on PM Emissions from a Light-Duty GDI Vehicle," *Aerosol Science and Technology* 46(5):576-583, 2012. DOI:10.1080/02786826.2011.648780. http://www.tandfonline.com/doi/abs/10.1080/02786826.2011.648780
23. He, X., Ratcliff, M.A., and Zigler, B.T., "Effects of Gasoline Direct Injection Engine Operating Parameters on Particle Number Emissions," *Energy Fuels* 26(4):2014-2027, 2012. dx.doi.org/10.1021/ef201917p. http://pubs.acs.org/doi/pdf/10.1021/ef201917p
24. Anderson, J.E., DiCicco, D.M., Ginder, J.M., Kramer, U., et al., "High Octane Number Ethanol-Gasoline Blends: Quantifying the Potential Benefits in the United States," *Fuel* 97:585-594, 2012. doi:10.1016/j.fuel.2012.03.017. http://www.sciencedirect.com/science/article/pii/S0016236112002268
25. Stein, R., Anderson, J., and Wallington, T., "An Overview of the Effects of Ethanol-Gasoline Blends on SI Engine Performance, Fuel Efficiency, and Emissions," *SAE Int. J. Engines* 6(1):470-487, 2013, doi:10.4271/2013-01-1635.
26. U.S. Department of Energy, 2011. *U.S. Billion-Ton Update: Biomass Supply for a Bioenergy and Bioproducts Industry*, Perlack R.D. and Stokes B.J. (Leads), Technical Report ORNL/TM-2011/224. Oak Ridge National Laboratory, Oak Ridge, TN. 227p.
27. Humbird, D., Davis, R., Tao, L., Kinchin, C., et al., *Process Design and Economics for Biochemical Conversion of Lignocellulosic Biomass to Ethanol Dilute-Acid Pretreatment and Enzymatic Hydrolysis of Corn Stover*, (Golden, CO: National Renewable Energy Laboratory) Technical Report NREL/TP-5100-47764, May 2011.
28. Arbogast, S., Bellman, D., Paynter, J.D., and Wykowski, J., "Advanced Bio-Fuels from Pyrolysis Oil: The Impact of Economies of Scale and Use of Existing Logistic and Processing Capabilities," *Fuel Proc. Techn.* 104:121-127, 2012. doi:10.1016/j.fuproc.2012.04.036. http://www.sciencedirect.com/science/article/pii/S0378382012001658
29. Arbogast, S., Bellman, D., Paynter, J.D., and Wykowski, J., "Advanced Biofuels from Pyrolysis Oil…Opportunities for Cost Reduction," *Fuel Proc. Techn.* 106:518-525, 2013. doi:10.1016/j.fuproc.2012.09.022. http://www.sciencedirect.com/science/article/pii/S0378382012003384
30. Talmadge, M.S., Baldwin, R.M., Biddy, M.J., McCormick, R.L., et al., "A Perspective on Oxygenated Species in the Refinery Integration of Pyrolysis Oil," *Green Chem.* 16:407-453, 2014. DOI: 10.1039/C3GC41951G. http://pubs.rsc.org/en/content/articlelanding/2014/gc/c3gc41951g#!divAbstract
31. Christensen, E., Chupka, G., Luecke, J., Alleman, T.L., et al., "Analysis of Oxygenated Compounds in Hydrotreated Biomass Fast Pyrolysis Oil Distillate Fractions," *Energy Fuels* 25:5462-5471, 2011. dx.doi.org/10.1021/ef201357h. http://pubs.acs.org/doi/pdf/10.1021/ef201357h
32. Alonso, D.M., Bond, J.Q, and Dumesic, J.A. "Catalytic Conversion of Biomass to Biofuels," *Green Chem.* 12:1493-1513, 2010. DOI: 10.1039/C004654J. http://pubs.rsc.org/en/Content/ArticleLanding/2010/GC/c004654j#!divAbstract
33. Roman-Leshkov, Y., Barrett, C.J., Liu, Z.Y., and Dumesic, J., "Production of Dimethylfuran for Liquid Fuels from Biomass-Derived Carbohydrates," *Nature* 447:982-986, 2007. doi:10.1038/nature05923. http://www.nature.com/nature/journal/v447/n7147/full/nature05923.html
34. Huber, G., Iborra, S., and Corma, A., "Synthesis of Transportation Fuels from Biomass: Chemistry, Catalysts, and Engineering," *Chem. Rev.* 106(9):4044-4098, 2006. DOI: 10.1021/cr068360d. http://pubs.acs.org/doi/abs/10.1021/cr068360d
35. Higashide, W., Li, Y., Yang, Y., and Liao, J.C., "Metabolic Engineering of *Clostridium Cellulolyticum* for Isobutanol Production from Cellulose," *Appl. Environ. Microbiol.* 77(8):2727-2733, 2011. doi: 10.1128/AEM.02454-10. http://aem.asm.org/content/77/8/2727.abstract

36. McCormick, R.L., Ratcliff, M., Christensen, E., Fouts, L., et al., "Properties of Oxygenates Found in Upgraded Biomass Pyrolysis Oil as Components of Spark and Compression Ignition Engine Fuels," *Energy Fuels* 29(4):2453-2461, 2015. DOI: 10.1021/ef502893g. http://pubs.acs.org/doi/abs/10.1021/ef502893g
37. Chupka, G., Christensen, E., Fouts, L., Alleman, T. et al., "Heat of Vaporization Measurements for Ethanol Blends Up To 50 Volume Percent in Several Hydrocarbon Blendstocks and Implications for Knock in SI Engines," *SAE Int. J. Fuels Lubr.* 8(2):251-263, 2015, doi:10.4271/2015-01-0763.
38. Perry, R.H., and Green, D.W., *Perry's Chemical Engineers' Handbook.* 7th ed. (McGraw-Hill, 1999). 2-346.
39. API Technical Data Book - Petroleum Refining, (Washington, DC: American Petroleum Institute Publishing Services, 1993.)
40. Yaws, C.L., *Yaws' Handbook of Thermodynamic and Physical Properties of Chemical Compounds: Physical, Thermodynamic and Transport Properties for 5,000 Organic Chemical Compounds*. (McGraw-Hill, 2003).
41. National Instruments, Combustion Analysis System Software for LabVIEW User Manual, pg 162. http://digital.ni.com/manuals.nsf/websearch/C2B04021AA306BBB86257BCD007365C6
42. AAM, Alliance of Automobile Manufacturers North American Fuel Survey, 2011.
43. Chickoos, J.S., and Acree, W.E., "Enthalpies of Vaporization of Organic and Organometallic Compounds, 1880-2002," *J. Phys. Chem. Ref. Data* 32(2):519-878, 2003. http://dx.doi.org/10.1063/1.1529214
44. Christensen, E., Yanowitz, J., Ratcliff, M., and McCormick, R.L., "Renewable Oxygenate Blending Effects on Gasoline Properties," *Energy Fuels* 25:4723-4733, 2011. dx.doi.org/10.1021/ef2010089. http://pubs.acs.org/doi/pdf/10.1021/ef2010089
45. API Technical Data Book - Petroleum Refining, API, 1993.
46. Material Safety Data Sheet, www.sigmaaldrich.com, accessed December 14, 2014.
47. Amer, A., Babiker, H., Chang, J., Kalghatgi, G. et al., "Fuel Effects on Knock in a Highly Boosted Direct Injection Spark Ignition Engine," *SAE Int. J. Fuels Lubr.* 5(3):1048-1065, 2012, doi:10.4271/2012-01-1634.
48. Chen, L., and Stone, R., "Measurement of Enthalpies of Vaporization of Isooctane and Ethanol Blends and Their Effects on PM Emissions from a GDI Engine," *Energy Fuels* 25:1254-1259, 2011. dx.doi.org/10.1021/ef1015796. http://pubs.acs.org/doi/pdf/10.1021/ef1015796
49. Ratcliff, M., Luecke, J., Williams, A., Christensen, E., et al., "Impact of Higher Alcohols Blended in Gasoline on Light-Duty Vehicle Exhaust Emissions," *Environ. Sci. Technol.* 47(23):13865-13872, 2013. DOI: 10.1021/es402793p. http://pubs.acs.org/doi/abs/10.1021/es402793p
50. Pecullan, M., Brezinsky, K., and Glassman, I., "Pyrolysis and Oxidation of Anisole near 1000 K," *J. Phys. Chem. A* 101(18):3305-3316, 1997. DOI: 10.1021/jp963203b. http://pubs.acs.org/doi/abs/10.1021/jp963203b
51. Scheer, A.M., Mukarakate, C., Robichaud, D.J., Ellison, G.B., et al., "Radical Chemistry in the Thermal Decomposition of Anisole and Deuterated Anisoles: An Investigation of Aromatic Growth," *J. Phys. Chem. A* 114(34):9043-9056, 2010. DOI: 10.1021/jp102046p. http://pubs.acs.org/doi/abs/10.1021/jp102046p

CONTACT INFORMATION

Matthew Ratcliff
matthew.ratcliff@nrel.gov

ACKNOWLEDGMENTS

This work was supported by the U.S. Department of Energy, Vehicle Technologies Office, under Contract No. DE347AC36-99GO10337 with the National Renewable Energy Laboratory, and was awarded under Funding Opportunity Announcement DE-FOA-0000239. The U.S. Government retains and the publisher, by accepting the article for publication, acknowledges that the U.S. Government retains a nonexclusive, paid-up, irrevocable, worldwide license to publish or reproduce the published form of this work, or allow others to do so, for U.S. Government purposes.

DEFINITIONS/ABBREVIATIONS

2-PE - 2-phenylethanol

4-MA - 4-methylanisole

BTDC - before top dead center

CAD - crank angle degree

DBE - double bond equivalent

DHA - detailed hydrocarbon analysis

DI - direct injection

DISI - direct injection spark ignition

DMF - 2,5-dimethylfuran

Exx - percent ethanol

FMPS - fast mobility particle sizer

HoV - heat of vaporization

KI - integrated knock, or knock-integral

KLSA - knock limited spark advance

MBT - minimum advance for best torque

MON - motor octane number

NMEP - net mean effective pressure

OI - octane index

PM - particulate matter

PMI - particulate matter index

PN - particle number

RON - research octane number

rpm - revolutions per minute

S - octane sensitivity (RON - MON)

SI - spark ignition

T50 - temperature at 50% distilled

T90 - temperature at 90% distilled

THC - total hydrocarbons

wt% - percent by weight